

HR Photometry of M55

Introduction and Theory:

HR diagrams, or color-magnitude diagrams (CMDs) have been used by astronomers starting in the 20th century to determine the age and composition of various clusters of stars. These clusters are ideal for generating HR diagrams because stars that are grouped closer together are more likely to show the progression of stellar evolution. For this project we chose to create an HR diagram of the M55 star cluster (NGC 6809). M55, apparent magnitude +6.7, RA(J2000) 19h 39m 59s, DEC(J2000) -30° 57m 44s, is a moderately bright and metal-poor halo cluster that makes a suitable candidate for photometric CMDs. BV CMDs have been done on M55 for several decades, and a study in 1992 was done on additional passbands R and I. The first few studies on M55 were conducted in the 1970s in only the B and V bands. The first in 1975 used 312 stars in the $12 < V < 18$ magnitude range. Another study in 1975 used 555 stars in the $11 < V < 16$ magnitude range. Both found an extremely blue horizontal branch in the ranges of $14.2 < V < 15.6$ and $-0.1 < B - V < 0.2$. A study in 1977, calibrated by about 4 times the number of stars than the initial two studies, used 512 stars with a magnitude range of $11 < V < 16$. In that final CMD, the blue horizontal branch was better defined in addition to the asymptotic branches. (Alcaino, G, et al. 1992)

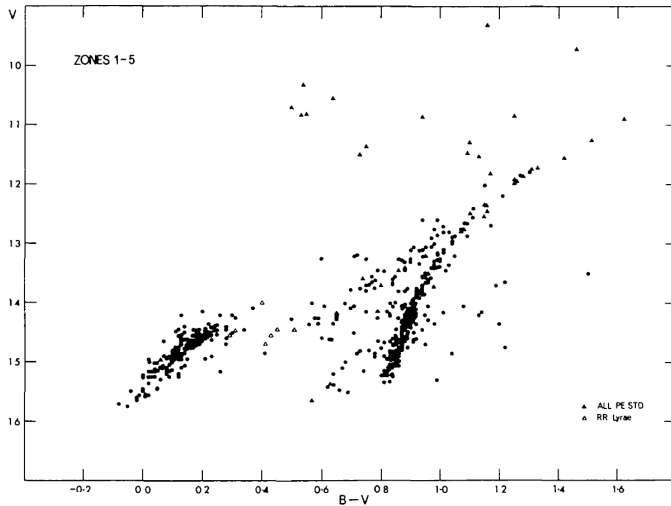


Figure 1 The CMD of M55. All measured stars in zones 1–5 are plotted including RR Lyrae variables (open triangles) and pe stars (filled triangles).

Figure 1 shows the CMD of M55 published by SW Lee in 1977. It plots all the stars identified in regions 1-5 in the chart of figure 2. Lee describes a gap at $V=14.8$ and $(B-V)=0.14$ as an unclear color boundary.

They mention the possibility of improving this gap by adding more blue stars to the study and having more accurate photometric

photometry of the inner stars. The paper also mention that the accuracy of the branches' spa-

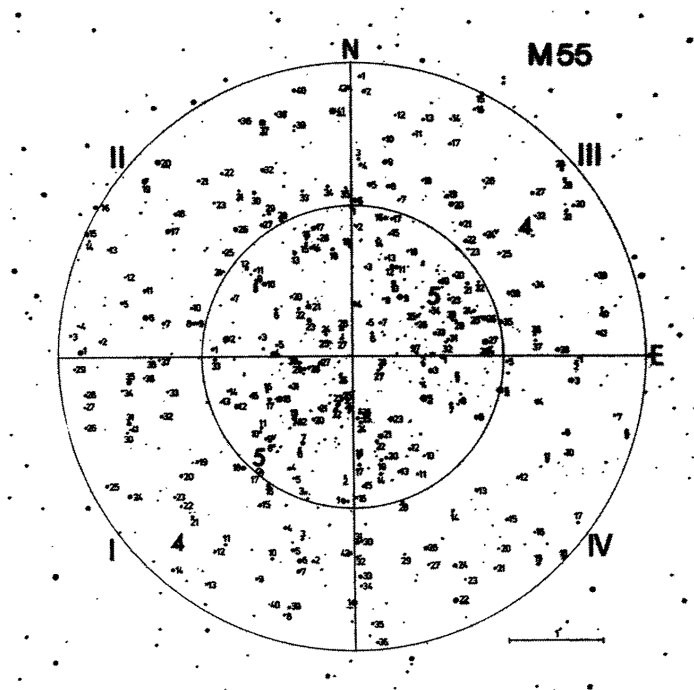


Figure 2 Finding chart (reproduction of 40 min. exposure V plate) for the photographic measurements of stars in the inner region of M55. The inner region is divided into two zones at intervals of 1.5 arcmin and into four quadrants. Others are the same as in figure 3.

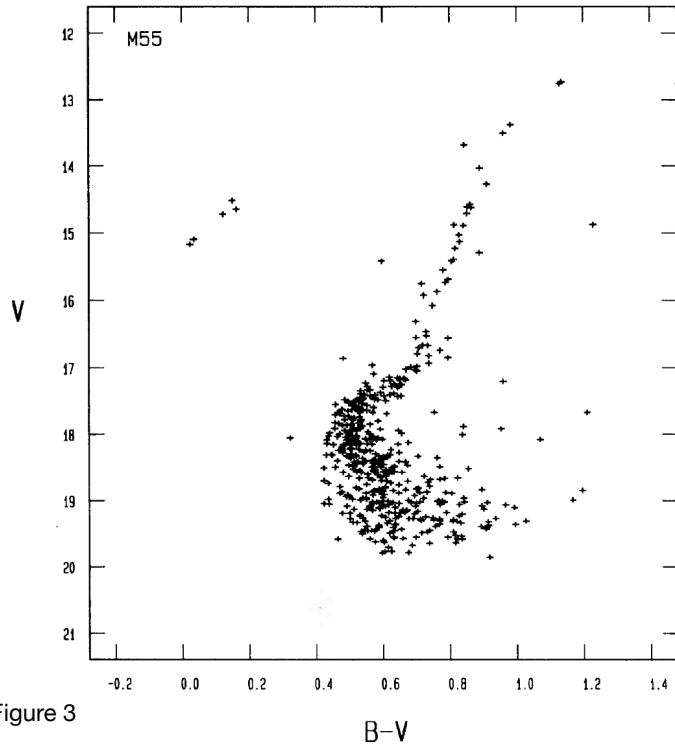


Figure 3

cial distribution cannot be assessed due to the incomplete measurements of the inner zone of stars.

Figure 3 shows the B-V CMD done by Alcaïno, G, et al. in 1992 with a 2.2m telescope and CCD, looking at 600 stars, 24 of which were found to be in common with the work of Lee. The images taken for this study were processed using the DAOPHOT stellar photometry package. I was unable to examine the source code or attempt to run a

form of the software. The general idea of the software can be compared to the DAOSTarFinder component of the Photutils package.

During my initial research, I came across a methodology for improving the signal to noise ratio (SNR) when imaging for the purpose of HR diagrams mentioned in a paper from 2008. In it they describe using a method called 2x2 binning for CCD imaging. This method allows for the charges on multiple pixels to be combined for a faster readout and higher SNR, while only sacrificing spacial resolution. If we were to compare this method to single pixel readout on a 2x2 pixel array, the main difference is that the charge on each pixel stays the same as the charges are shifted to the readout register. The binning method, on the other hand, will sum up all the charges in the readout amplifier before readout. By summing the 4 pixels values into one, readout time is twice as fast and with higher pixel numbers would only get faster. In addition,

SNR also turns out to be twice as good. This method is very useful in applications like spectroscopy where spectral lines are slits that will show up on the CCD with a very high aspect ratio and can be binned for optimal SNR without losing spectral resolution. (Yadav, R. K. S. et al.)

According to data from the LCO .fits files, our images only used 1x1 binning.

The method for creating our HR diagram intended on following this procedure: After two images have been taken, one with a B filter and one with a V filter (both corrected appropriately), several reference stars need to be matched with a chart in order to calibrate the software being used to measure the magnitude of a chosen group of stars. The magnitude for these stars needs to be determined in the B and V images separately. Once the software is calibrated, m_V can be used to find m_B with an accurate B-V index for that star. Once that is complete the B-magnitudes can be calibrated. After using the software to get as many values for m_V and m_B the B-V indices need to be calculated for all of the stars. Next m_V is plotted on the y-axis, while the B-V index is on the x-axis. This gives us a plot of luminosity over surface temperature and forms the HR diagram. In the case of a cluster that is in an area of high dust content, a correction may be needed. Dust will make stars appear redder, so the diagram will need an appropriate adjustment. If the image was taken from the ground on Earth, an air mass correction is needed as well.

Historical Background:

The first observations of the H-R diagrams came in 1905 by Ejnar Hertzsprung and in 1910 by Henry Norris Russell. The purpose of their work was to find the meaning of the differences found in stars' spectra. After plotting the relationship between stellar energy output against surface temperature, both researchers realized that for most stars on the main diagonal of the plot

the fainter they are, the more red they are compared to the brighter ones. But the group of stars found at the top right of the diagram didn't share the same correlation. The ability to discern the qualities that made some stars giants and others dwarfs was a challenge for 19th century astronomers that was based on fundamental assumptions of the nature of stars. Astronomers initially concluded that only the process of converting mechanical energy into heat could be responsible for stellar evolution. This led to an assumption that the cooling process could be observed by looking at the spectral differences between stars. The first classifications were based on blue stars as the hottest, youngest stars transitioning to yellow, then red, then extinction. But some astronomers found that there were significant differences within the classes themselves. Some, like J. Norman Lockyer, believed that the two distinct classes of red stars suggested two periods of their evolution in which they were red, the beginning and end. Though his observations were initially challenged, later research by J. Homer Lane and August Ritter gave the theoretical support needed to gain Lockyer attention. At the time, however, photographic technology and spectral resolution issues prevented any classification systems from producing consistent results. The quality of observations drastically changed when E.C. Pickering took the position of director of the Harvard College observatory in 1877. Pickering used objective prisms placed in front of wide-field photographs, providing him with the spectra of hundreds of stars from just one photograph. With the help of a team of women headed by Wilhaminia P. Flemming, Pickering and Flemming created the Draper Catalogue of Stellar Spectra with around 10,000 stars. Initially, Pickering's classification consisted of letters A,O,P and Q, based on the visibility of hydrogen spectral lines. With the help of Annie C. Cannon, the order of classifications was modified due to additional spectral and the similarity in helium lines between classes. The resulting classification

was O, B, A, F, G, K, M. Although part of the standard classification we use today, it was already determined at the time that this system was still rough at best. In 1897 Antonia Maury had been tasked with developing a more sophisticated classification system. Her system was not only 22 numerical groups, but subdivided the classes into two groups. These two groups separated stars with broad hydrogen lines, and stars with sharp hydrogen lines and accentuated metallic lines. She proposed that these distinctions suggested “parallel courses of development”. Though her work would be revisited by Hertzsprung when looking at the physical properties of stars, Maury’s work was largely unnoticed initially. When Hertzsprung began his work, he used proper motions of stars to statistically derive relative distances and brightness for different spectral classes. This wasn’t unlike researchers before him other than the fact that he was intrigued by Maury’s separation of classifications. By using the analysis of proper motion, he was able to distinguish bright and faint red stars depending on the categories of proper motion and brightness they fell into. Henry Norris Russell, on the other hand, had been focused on the hypothesis of Lockyer. After conducting his own research mimicking Lockyer’s, but with less of a reliance on the brightness of stars for selection, Russell began to make conclusions that sounded very similar to those of Hertzsprung. Both Hertzsprung and Russell had independently come to similar conclusions about the relationship of stars’ spectra and brightness before the HR diagram had truly been developed. The HR diagram existed to some extent before the conclusions had ever been made, but it was ultimately those two researchers who finalized the interpretation of the diagrams. Today, there have been refinements to interpreting data in this way as the quality of data has improved, and researchers continue to observe various stellar objects to improve the accuracy of their conclusions. (Devorkin 1978)

Larger context of importance:

When we look at stars from the earth or a space-based telescope, we are limited by our inability to travel to any of those stars to verify our calculations. This inevitably leads to an issue of accounting for any forms of error, and creating the most accurate models possible. The HR diagram provides a basis for how we look at the universe around us. Accurate determinations of age for the star clusters we observe allow us to make conclusions about the formation and evolution of stars and the methods ultimately aid in the determination of the age of the universe.

Data Collection and any issues:

Image capture was the first and simplest step to perform, but a difficult step to refine. We requested two images using the Bessel B and Bessel V filters, each at 100 second integration times. The first issue we encountered was getting our program to detect enough stars that could be referenced between both images and compared to known values. We struggled for some time getting some of the brightest stars to be detected in both images. Once we could detect a favorable number of stars, alignment was our next challenge. The shift between images wasn't large, but the program could not match the stars between images. Initially we attempted processing the images with AstroArt, lining them up, and then exporting the images, but the program gave us additional issues when we tried opening up the .fits files. The final reads the .fits header to pull the data. A background median is created to isolate only the stars in the images. A chosen number (nb) determines how many of the brightest stars in the image are searched for. Next, a mask is created by selecting 4 stars manually that could be found on both images, which creates a square mask that helps to align the images. An average is then calculated for the difference in X and Y coordinates between images in order to find the translational shift of the images. Minimal rota-

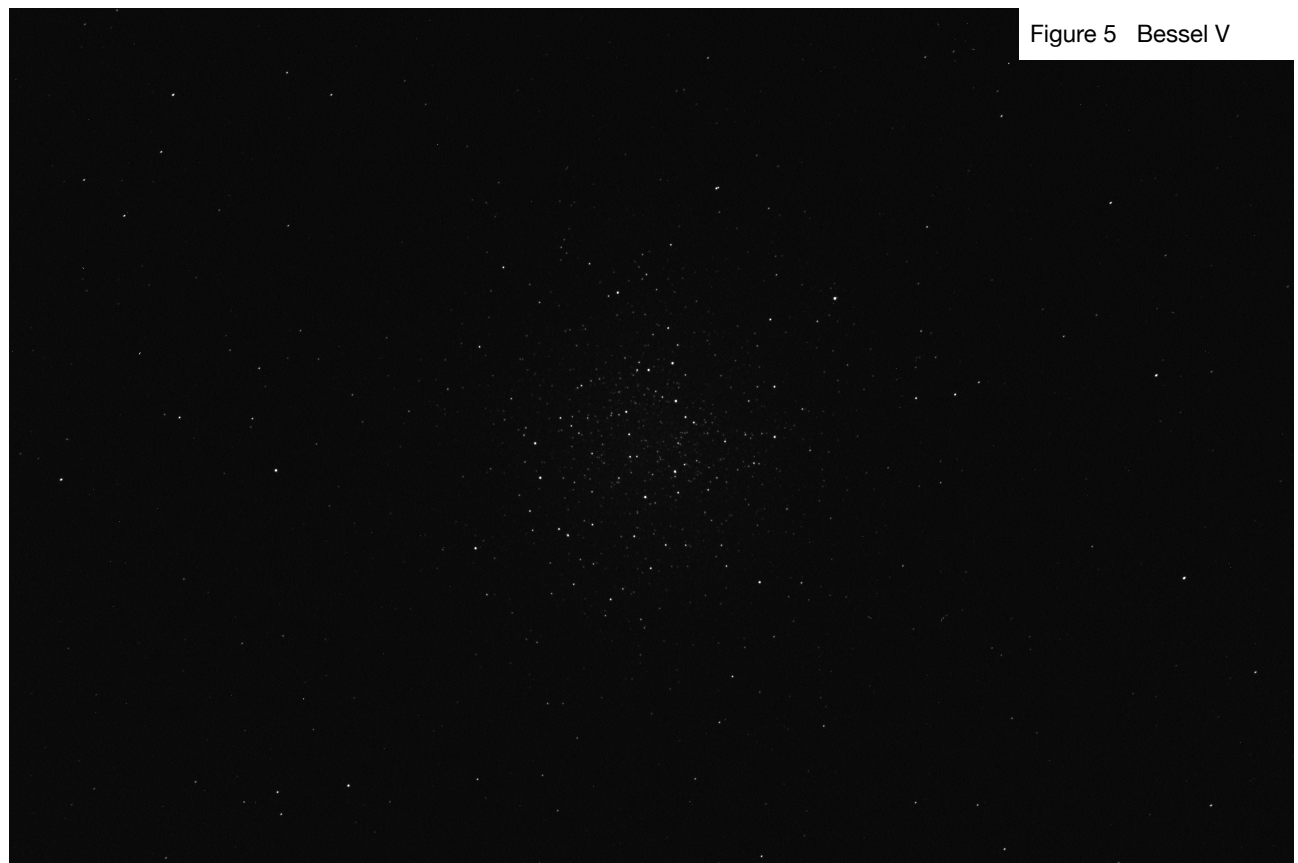
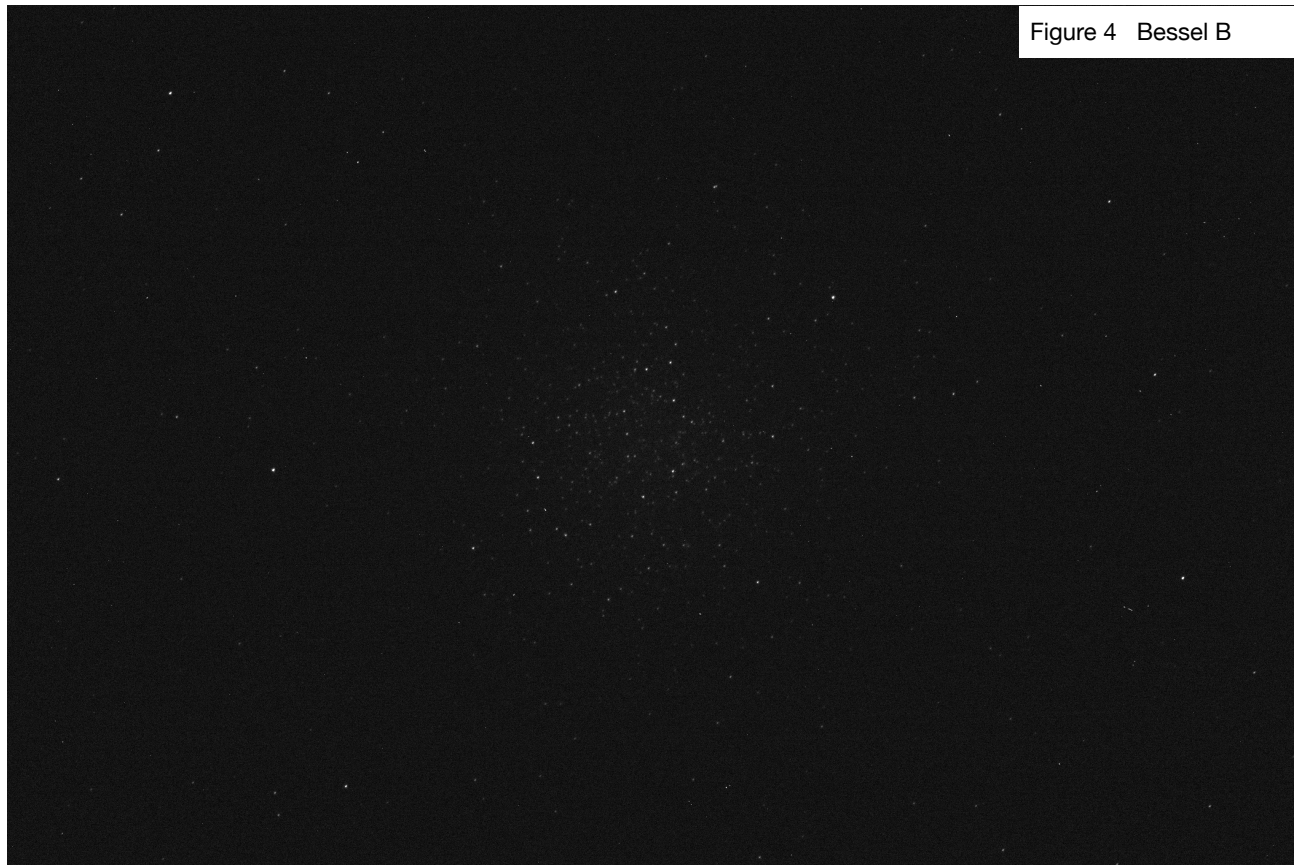


Figure 6 Bessel B Data Generated

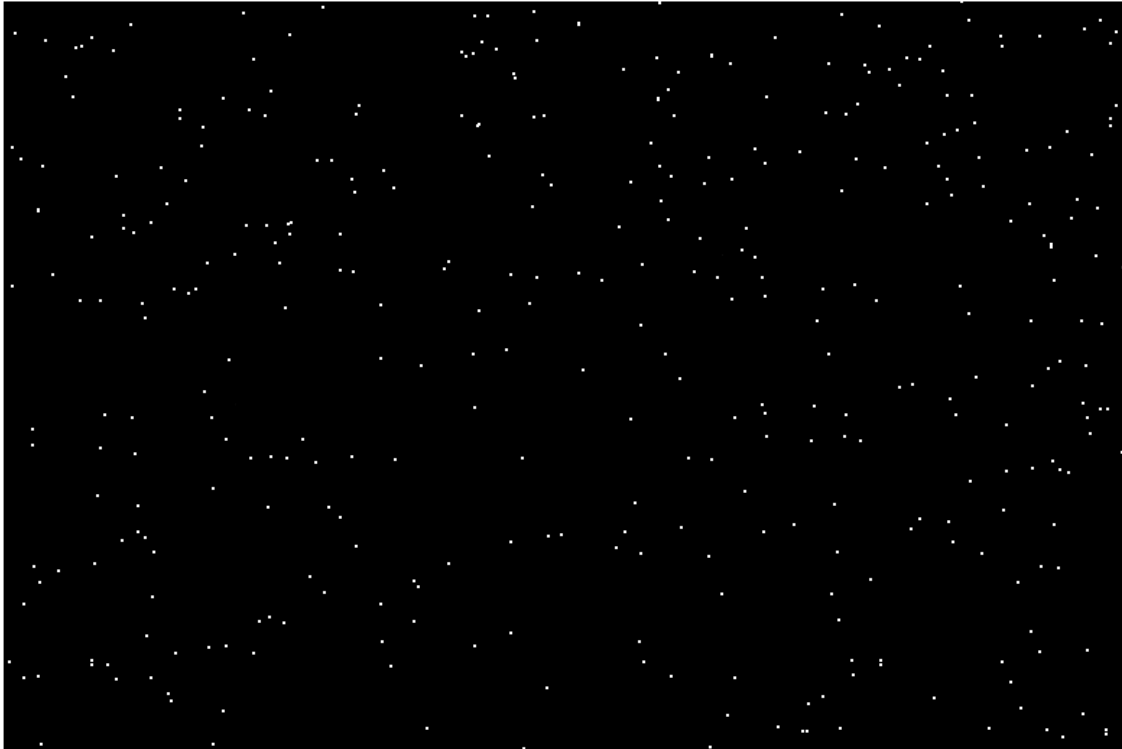
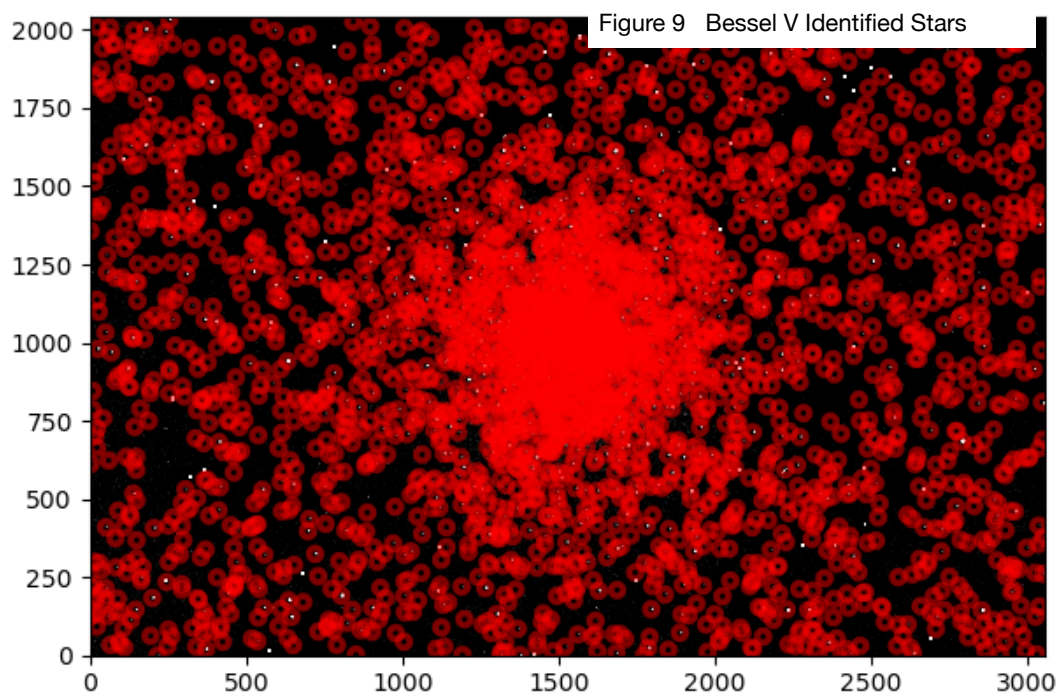
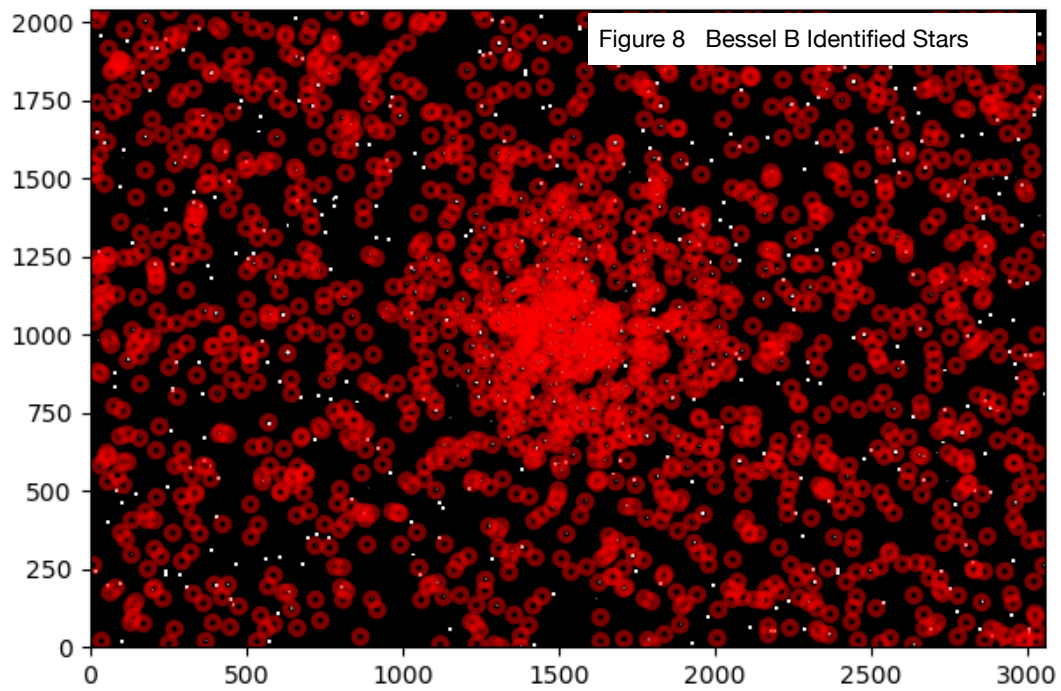


Figure 7 Bessel V Data Generated





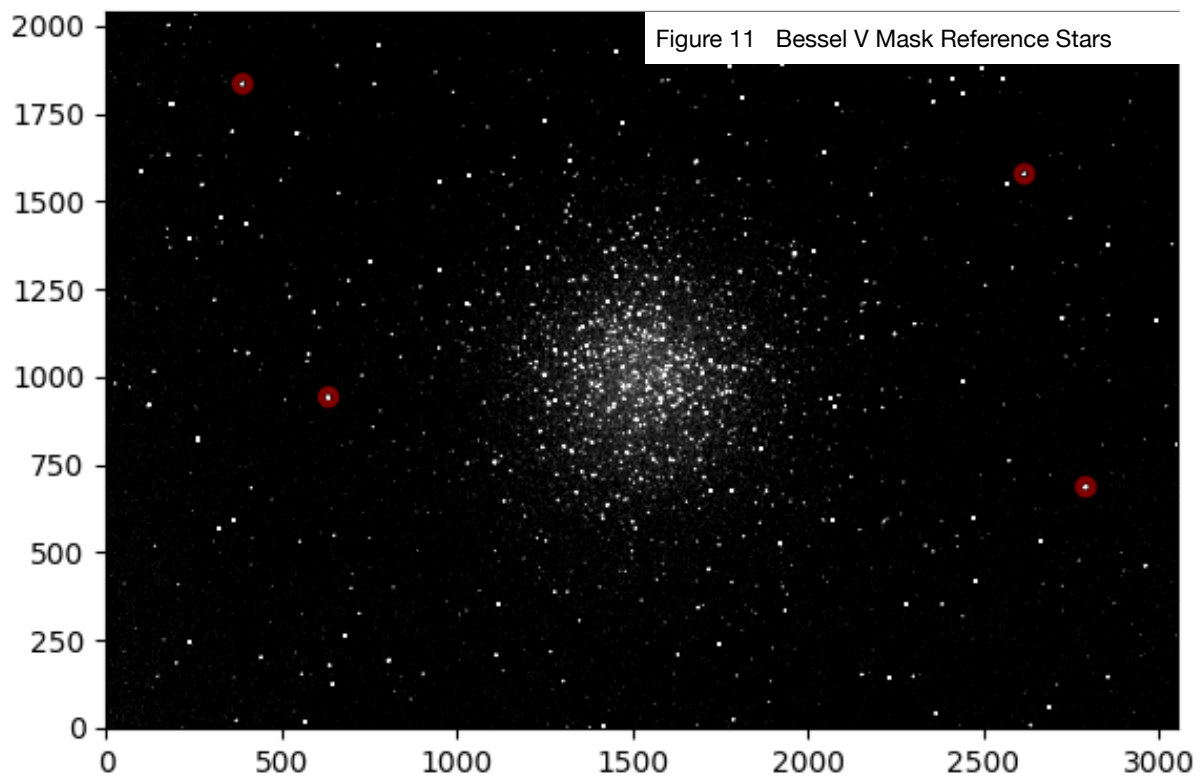
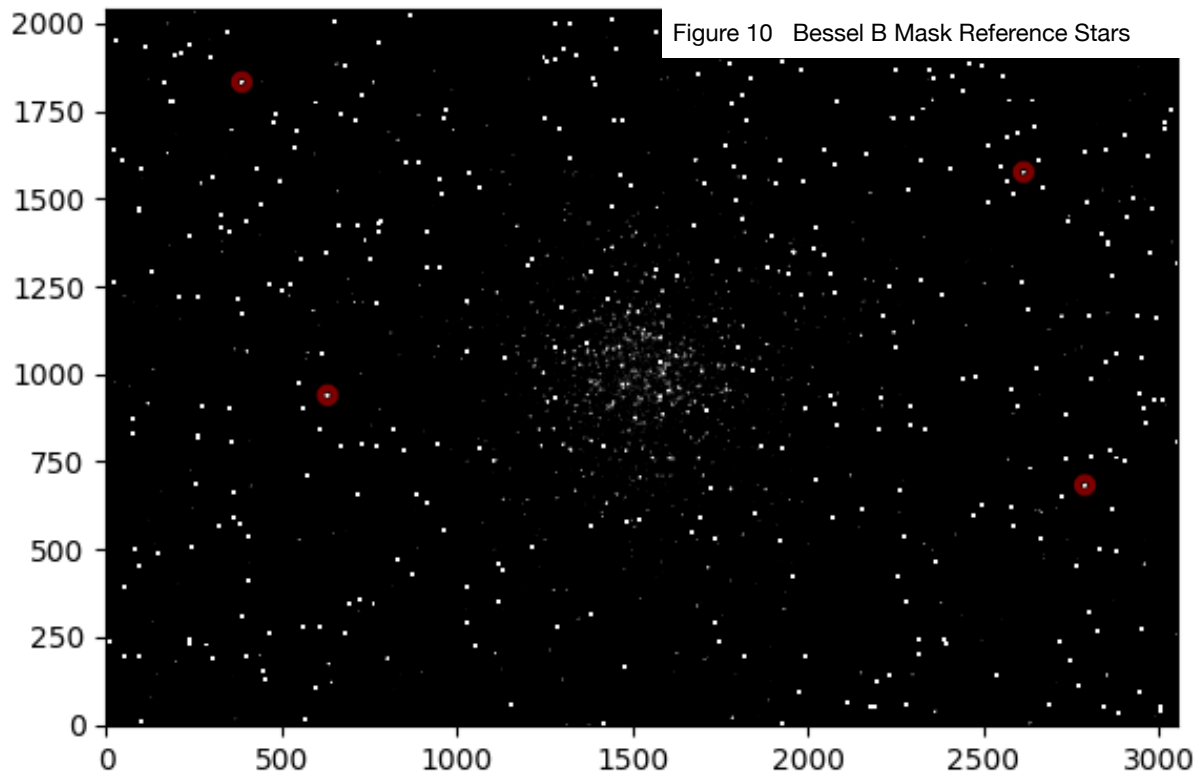


Figure 12 Initial Diagram nb=1000

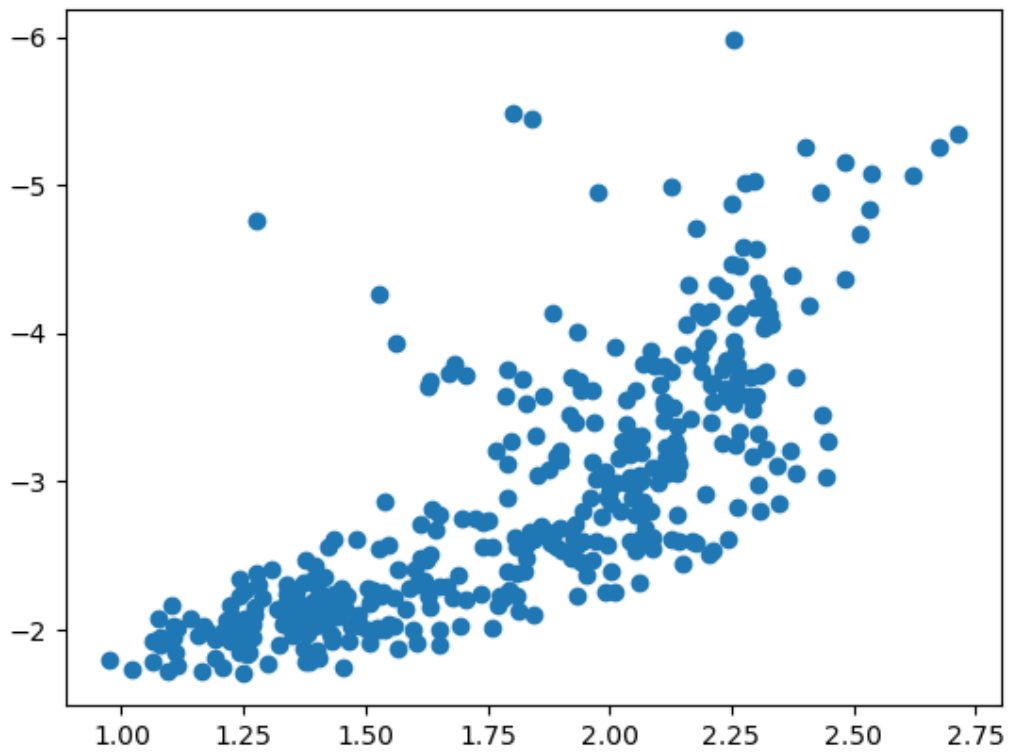
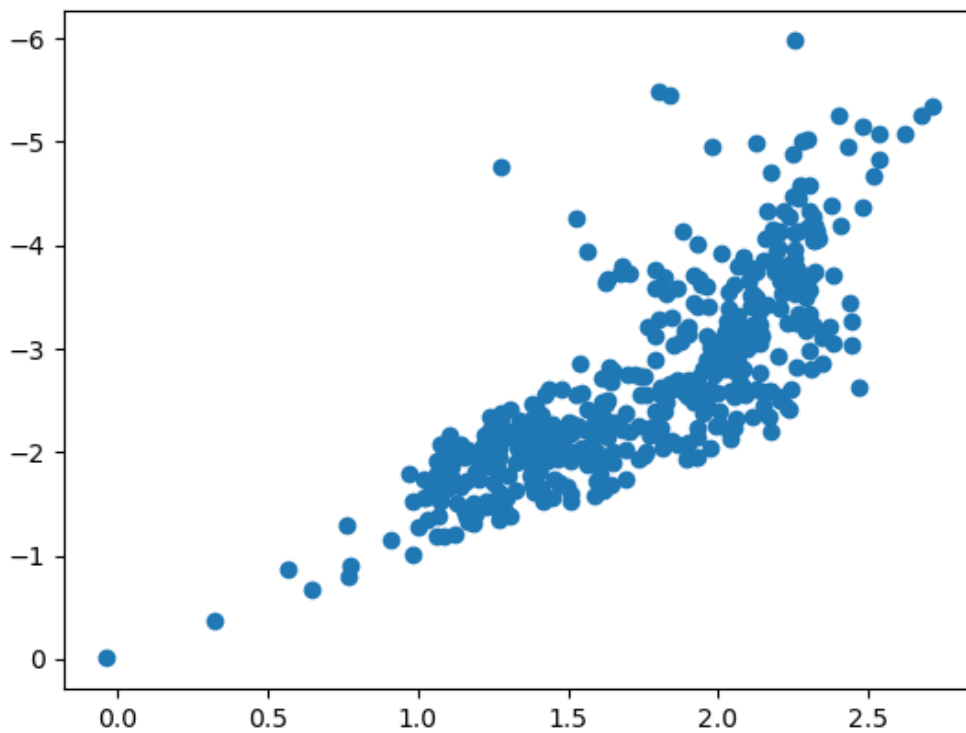
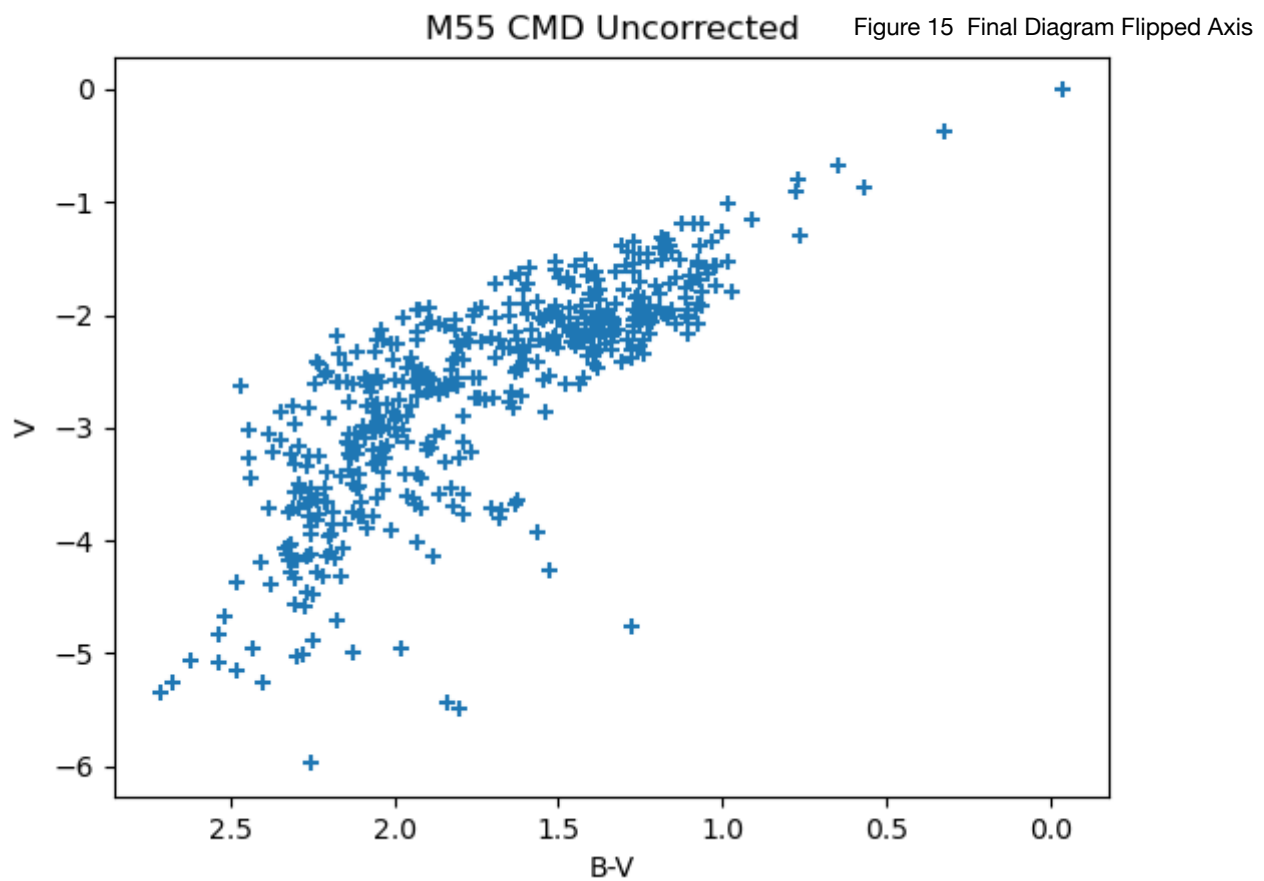
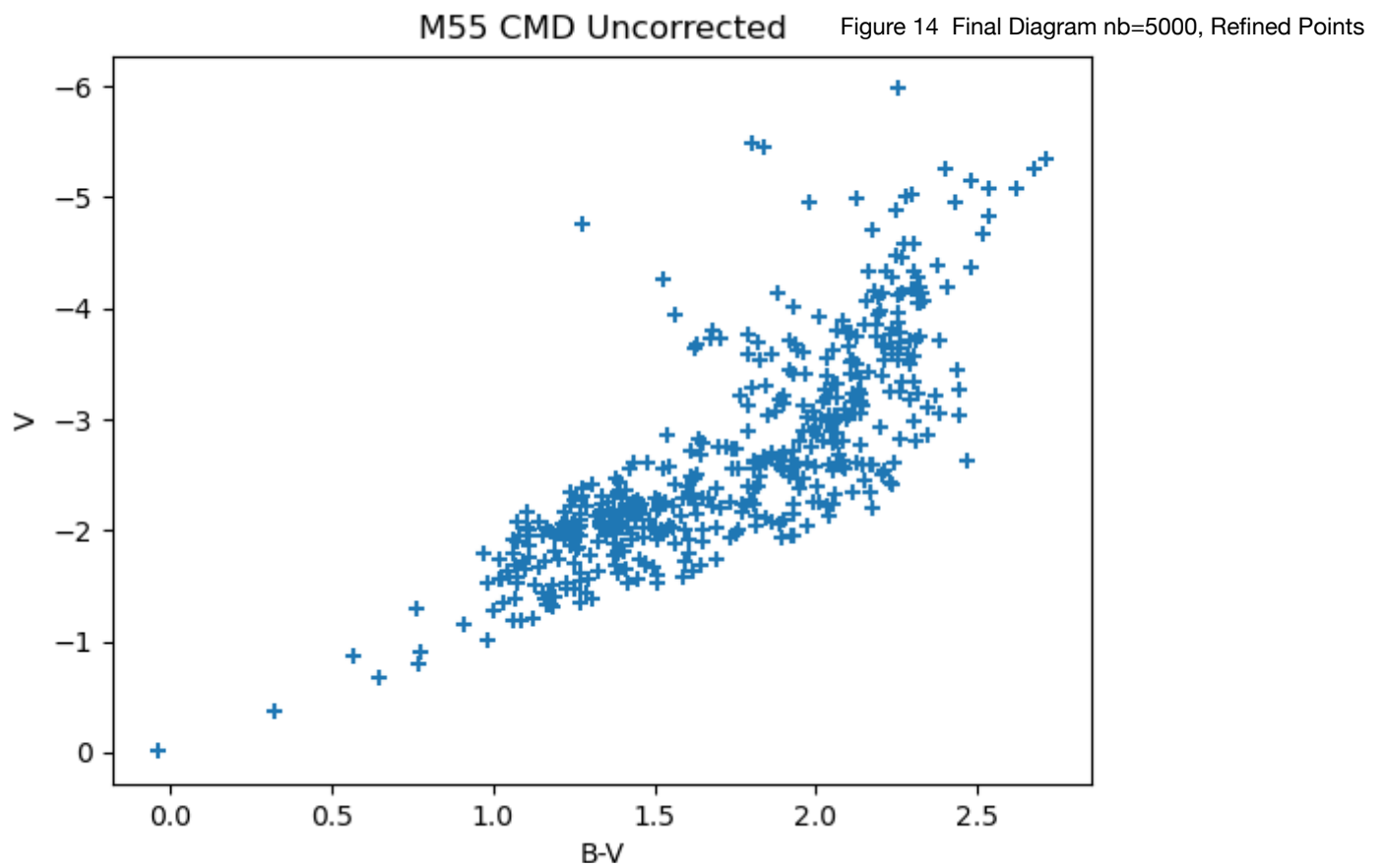


Figure 13 Second Diagram nb=5000





tional shift was found so it was not applied in this program. After the alignment is corrected, the program sweeps through the corrected list of stars and uses a threshold value for the distance between stars to match the stars between images and create a new list. After the list is created the diagram can be plotted, with the Y axis inverted for the magnitude.

Images and Plots Descriptions:

Figures 4 and 5 are the initial images of M55 received from LCOs SBIG .4m telescope through the Bessel B and Bessel V filters respectively. After putting the images into our program, figures 6 and 7 show the interpretation of the images through the software when the image data is plotted. Figures 8 and 9 show the selection of the stars using DAOSTarfinder.

```
def find_sources_DAO (image_data, FWHM, thresh, sharphi, mask, nb):
    mean, median, std = sigma_clipped_stats(image_data, sigma=3.0)
    daofind = DAOSTarFinder (fwhm= FWHM, threshold= thresh*std, sharphi= sharphi, brightest= nb)
    sources_B = daofind (image_data - median, mask = mask)
    return (sources_B)

positions = np.transpose((sources_B['xcentroid'], sources_B['ycentroid']))
apertures = CircularAperture(positions, r=10)

positions_V = np.transpose((sources_V['xcentroid'], sources_V['ycentroid']))
apertures_V = CircularAperture(positions_V, r=10)
```

The excerpts of code above show the portions of our code that generate the plots for those figures. DAOSTarfinder essentially searches for gaussian distributions of magnitude in order to correctly distinguish random pixels from actual stars. There were still several stars that were not detected by the program, which we believe was due to shape properties of the stars. Figures 10 and 11 show the reference stars that were used to generate the mask that aligned the two images. The code below shows the process of finding the average difference in x and y distances that aligned the images:

```

def find_deltas (image_data_B, image_data_V):
    mask_calibration = np.ones (image_data_V.shape, dtype = bool)

    mask_default = np.zeros (image_data_B.shape, dtype = bool)
    mask_calibration[1810:1850, 370:410] = False
    mask_calibration[925:965, 615:655] = False
    mask_calibration[665:705, 2770:2810] = False #2790, 685
    mask_calibration[1560:1600, 2600:2640] = False #2620, 1577

    #print (mask_B[390,1830])

    sources_B = find_sources_DAO (image_data_B, 5, 3.5, 2, mask = mask_calibration, nb = 4)
    sources_V = find_sources_DAO (image_data_V, 5, 3.5, 2, mask = mask_calibration, nb = 4)

    #print ("calpix", header_B['CRIPIX1'])
    #sources_B = find_sources_DAO_invert (image_data, 5, 3.5, 2, mask = mask_default)
    #sources_V = find_sources_DAO_invert (image_data_V, 5, 3.5, 2, mask = mask_default)

    reference_list_B = [[x['xcentroid'] for x in sources_B],[y['ycentroid'] for y in sources_B]]
    reference_list_V = [[x['xcentroid'] for x in sources_V],[y['ycentroid'] for y in sources_V]]

    delta_x_list = [reference_list_B[0][i] - reference_list_V[0][i] for i in range(len(reference_list_B[0]))]
    delta_y_list = [reference_list_B[1][i] - reference_list_V[1][i] for i in range(len(reference_list_B[1]))]
    delta_x = np.mean (delta_x_list)
    delta_y = np.mean (delta_y_list)

    return (delta_x, delta_y)

```

Figure 12 is the diagram that was generated after the initial program was run, with the nb value chosen as 1000, finding roughly 400 stars. Figure 13 shows the diagram generated after changing the nb value to 5000, resulting in an additional 81 stars being found. Figure 14 shows our final HR diagram. After further evaluation, we should add that we were unable to match stars in our images to any reference stars in order to calibrate magnitudes. They were calculated instead by using the formula:

$$m = -2.5 \log^* \left(\frac{\text{peak density}}{\text{detection threshold}} \right)$$

This could potentially affect the B-V index and therefore the shape of the diagram.

Figure 15 shows one of the inversions of our diagram that we used when attempting to match our diagram to the previous studies of M55

Data Analysis:

After creating the final diagram from our data (Figure 14), we compared it to the existing diagrams of M55 found by previous studies. Based on the appearance of our diagram, we believe that we have isolated an area that can be seen in Figure 3 between $V=16$ and $V=17$, right before the main sequence turnoff point. In Figure 12 you can see less data below $V=-2$ than in the following figures. This is due to the initial code looking for far less stars to fit the threshold. In the code we initially had the “nb” value as 1000, and in the other two diagrams, we changed that value to 5000. The program found around 80 more stars when the value was increased. After determining the magnitude reference to be a source of error, we cannot be certain that our diagram matches any portion of more accurate diagrams found in previous studies. Without the reference, our B-V values could be quite skewed.

Error Analysis:

Extinction:

Though M55 was chosen for the qualities that make it a favorable photographic photometry object, there are certainly some sources of error that came into our research. We were unable to properly account for the effects of interstellar extinction. Interstellar dust can greatly affect the shift in observed wavelengths. As described in a paper by Fitzpatrick in 1998, there are several ways to account for extinction, each with their own considerations.

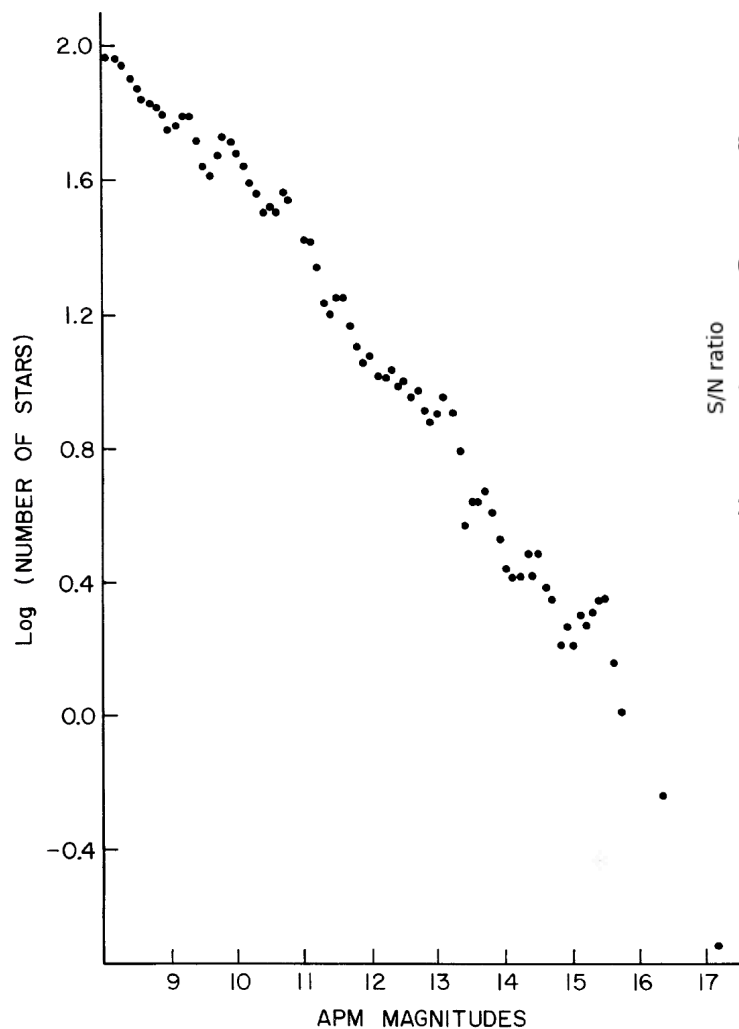


Figure 18 Background luminosity function, slightly smoothed, as used to analyze counts in the cluster. The residual statistical noise is sometimes reflected in the counts in Figs. 3 and 4. The magnitude range $APM = 8-17.2$ is equivalent to $J = 21.1-12.4$. Numbers are total numbers of images in bins $0.1 APM$ wide over the 263 sq min available for background determi

Figure 16 S/N ratio over magnitudes in the B band

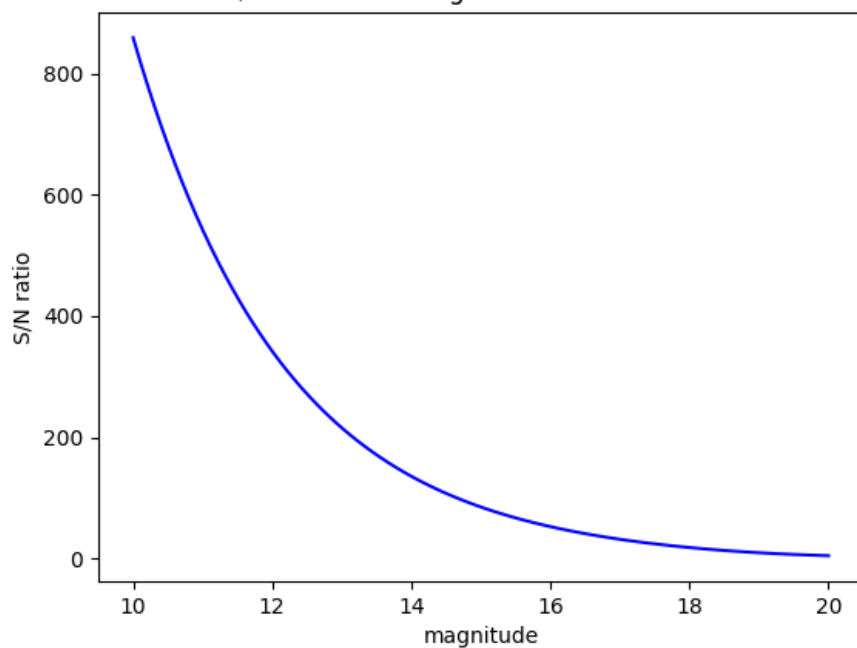


Figure 17 S/N ratio over magnitudes in the V band

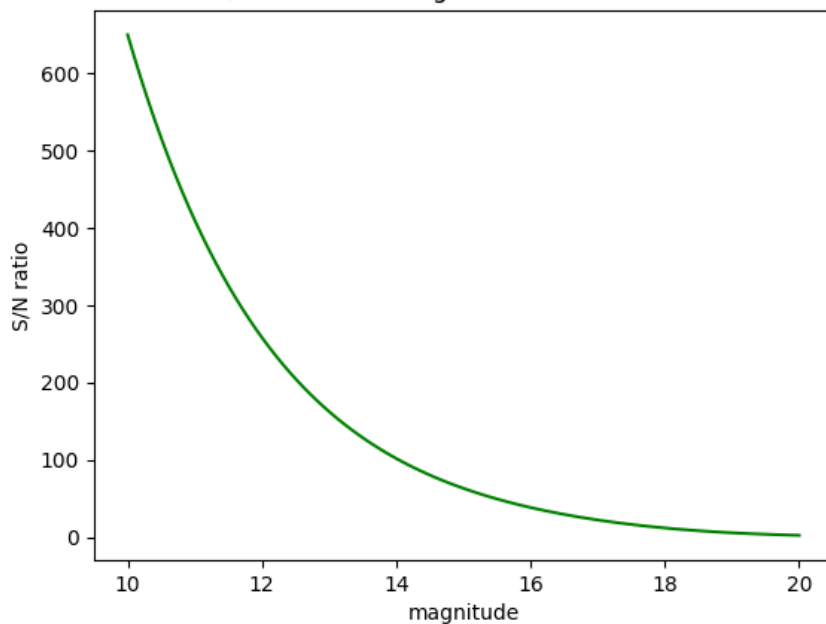


Figure 19 shows estimates of the Galactic extinction curve from far-IR through UV. The bump at 2175 \AA was discovered over 50 years ago using satellite and rocket spectrophotometric data. The IUE satellite provided a wealth of data for UV extinction along Winky Way lines of sight with its coverage of 1150 to 3200 \AA and a fairly high resolution. Though there is high spacial variability of extinction in the UV, Savage (1975) found that the 2175 \AA bump could be reproduced with a Lorentzian profile. Further mathematical models allowed researchers to create prediction curves that showed that spacial variations seen in extinction acted consistently across wavelengths, which would allow for uniform de-reddening for multi wavelength distributions. Considering the

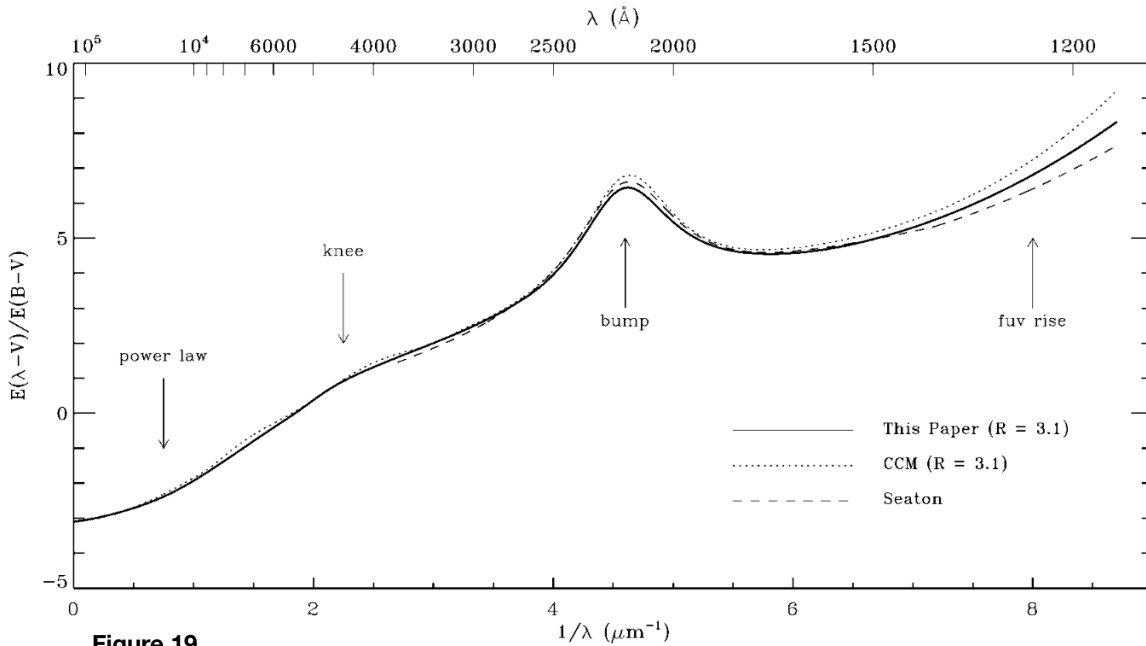


FIG. 1.—Normalized interstellar extinction curves from the far-IR through the UV. Several general features of the curves are noted. The solid and dotted curves are estimates for the case $R \equiv A(V)/E(B-V) = 3.1$ derived in the Appendix of this paper and by Cardelli et al. (1989), respectively. The dashed curve shows the average Galactic UV extinction curve from Seaton (1979).

possibility of this error, we knew it would be a factor in the accuracy of our data. Different studies on M55 showed variations of counteracting interstellar extinction. In the study by Schade et al. (1988), they suggest that the reddening could be as high as $E(B-V)=0.14$ based on previous

CMDs of M68 and NGC 6752. In the paper by Alcaïno et. al. (1992), they found reddening to be $E(B-V)=0.16 \pm 0.03$. Due to time constraints, we hadn't evaluated the reddening correction we wanted to use. Atmospheric extinction was another consideration in the effect on our images due to our observations being ground-based. One source I found showed an approximate shift of 0.15 for the V band and a shift of .3 for the B band. This was based on the specific location it made observations at but we were unable to find the appropriate atmospheric extinction chart for our observations.

Another clear example of error has been in the algorithm used to locate stars. We noticed that any available python-based star finder programs required a large amount of fine tuning in order to achieve any favorable results.

S/N and Equipment:

Figures 16 and 17 show the S/N calculated for each filter using a separate program that calculates the following:

$$\frac{S}{N} = \frac{FA_{\varepsilon} \sqrt{\tau}}{\left[\frac{N_R^2}{\tau} + FA_{\varepsilon} + i_{DC} + F_{\beta} A_{\varepsilon} \Omega \right]^{1/2}} = \frac{FA_{\varepsilon} \sqrt{\tau}}{\left[\frac{N_R^2}{\tau} + N_T \right]^{1/2}} = \frac{FA_{\varepsilon} \tau}{\left[N_R^2 + \tau N_T \right]^{1/2}}.$$

The significance of these calculations shows that we could not get reliable data points with magnitudes greater than about 19 due to the S/N being around 9 for the B band and 6 for the V band.

Figure 18 shows the drop-off of the number of stars detected as magnitude increases from the 1983 study from M. J. Irwin and V. Trimble.

Summary and Conclusions:

When using photometry to generate an HR diagram, there are several important considerations that need to be made. The first, and probably most important is that of the visibility of the chosen object. M55 was not a poor choice for the time frame we had to get data. However, by prioritizing the coding aspect of the project, we ran into an issue during the last few weeks. Tracking visibility for all locations of the available LCO telescopes ahead of our project would have removed any uncertainties for when we could request data. As previously mentioned, we had issue with the calibration of our data, which affected the overall visual reliability of our diagrams. Though it would be “nice” to believe that the data could look like some portion of previous diagrams of M55, ultimately we have to accept that all the observed forms of error created significant doubt. If we could approach this project again, there are several things we would have changed. The most obvious aspect of a project as longterm as this is the allocation of time and tasks. Creating a schedule for the goals we had throughout this project would have greatly impacted the depth that we could go. Having never accessed online databases for information as raw as stellar measurements, learning how to access and interpret these databases would have been useful earlier as well. If we could have taken more images, the availability of data would have improved our calculations once we began creating the program. Regarding the program we leaned heavily on one group member due to his python experience, and I would have preferred knowing what I know know about the coding concepts we ended up using. Overall, an interesting challenge.

Bibliography:

Alcaino, G, et al. "Bvri Ccd Photometry of the Globular-Cluster m55 (Ngc 6809)." *The Astronomical Journal*, vol. 104, no. 1, 1992, pp. 190–202., <https://doi.org/10.1086/116230>.

Devorkin, David H. "Steps toward the Hertsprung–Russell Diagram." *Physics Today*, vol. 31, no. 3, 1978, pp. 32–39., <https://doi.org/10.1063/1.2994966>.

Fitzpatrick, Edward L. "Correcting for the Effects of Interstellar Extinction." *Publications of the Astronomical Society of the Pacific*, vol. 111, no. 755, 1999, pp. 63–75., <https://doi.org/10.1086/316293>.

Irwin, M. J., and V. Trimble. "Automated Star Counts in the Southern Globular Cluster NGC 6809 (M55)." *The Astronomical Journal*, vol. 89, 1984, pp. 83–94., <https://doi.org/10.1086/113485>.

Lee, S. -W. "The C-M Diagram of The Globular Cluster M55." *Astronomy and Astrophysics, Suppl. Ser.*, Vol. 29, 1977, p. 1-8., <https://adsabs.harvard.edu/pdf/1977A%26AS...29....1L>

Nasibov, A, et al. "The Influence of CCD Pixel Binning Option to Its Modulation Transfer Function." *Spie-Int Soc Optical Engineering*, Vol. 7723, 2010, pp. 77231A–77231A-8. *Proceedings of SPIE*, <https://doi.org/10.1117/12.854738>.

Sandquist, Eric L, and Michael Bolte. "Exploring the Upper Red Giant and Asymptotic Giant Branches: The Globular Cluster M5." *The Astrophysical Journal*, vol. 611, no. 1, 2004, pp. 323–337., <https://doi.org/10.1086/422134>.

Schade et. al. "A Color-Magnitude Diagram For The Halo Globular Cluster M55." *Astronomical Journal* (ISSN 0004-6256), vol. 96, Nov. 1988, p. 1632-1641. 1988AJ.....96.1632S

Straizys, V. "From Multicolor Photometric Indices to the HR Diagram." *Symposium - International Astronomical Union*, vol. 80, 1978, pp. 293–300., <https://doi.org/10.1017/S0074180900145693>.

Yadav, R. K., et al. "Optical and near-Infrared Photometric Study of the Open Cluster NGC 637 and 957." *Monthly Notices of the Royal Astronomical Society*, vol. 390, no. 3, 2008, pp. 985–996., <https://doi.org/10.1111/j.1365-2966.2008.13740.x>.

"Las Cumbres Observatory Global Telescope Network", Brown, T. M. et al., Publications of the Astronomical Society of the Pacific, 2013, Volume 125, issue 931, pp.1031-1055